Inorganic Chemistry

Article

pubs.acs.org/IC

Reactivity of Compound II: Electronic Structure Analysis of Methane Hydroxylation by Oxoiron(IV) Porphyrin Complexes

Angela Rosa* and Giampaolo Ricciardi*

Dipartimento di Chimica, Università della Basilicata, Viale dell'Ateneo Lucano 10, 85100 Potenza, Italy

ABSTRACT: The methane hydroxylation reaction by a Compound II (Cpd II) mimic PorFe^{IV}=O and its hydrosulfide-ligated derivative [Por(SH)Fe^{IV}=O]$^-$ is investigated by density functional theory (DFT) calculations on the ground triplet and excited quintet spin-state surfaces. On each spin surface both the σ- and π-channels are explored. H-abstraction is invariably the rate-determining step. In the case of PorFe^{IV}=O the H-abstraction reaction can proceed either through the classic π-channel or through the nonclassical σ-channel on the triplet surface, but only through the classic σ-mechanism on the quintet surface. The barrier on the quintet σ-pathway is much lower than on the triplet channels so the quintet surface cuts through the triplet surfaces and a two state reactivity (TSR) mechanism with crossover from the triplet to the quintet surface becomes a plausible scenario for C−H bond activation by PorFe^{IV}=O. In the case of the hydrosulfide-ligated complex the H-abstraction follows a π-mechanism on the triplet surface: the σ* is too high in energy to make a σ-attack of the substrate favorable. The σ- and π-channels are both feasible on the quintet surface. As the quintet surface lies above the triplet surface in the entrance channel of the oxidative process and is highly destabilized on both the σ- and π-pathways, the reaction can only proceed on the triplet surface. Insights into the electron transfer process accompanying the H-abstraction reaction are achieved through a detailed electronic structure analysis of the transition state species and the reactant complexes en route to the transition state. It is found that the electron transfer from the substrate σ_{CH} into the acceptor orbital of the catalyst, the Fe−O σ* or π*, occurs through a rather complex mechanism that is initiated by a *two-orbital four-electron* interaction between the σ_{CH} and the low-lying, oxygen-rich Fe−O σ-bonding and/or Fe−O π-bonding orbitals of the catalyst.

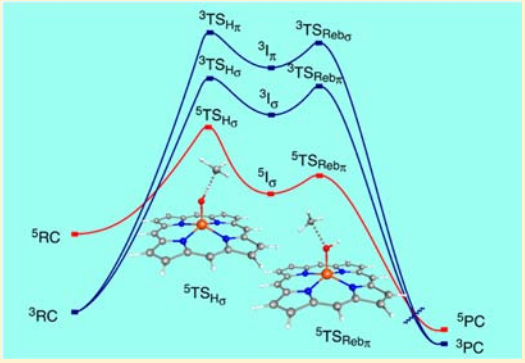

INTRODUCTION

Oxoiron(IV) species are invoked as key oxidizing intermediates in the catalytic cycles of heme[1] and non heme enzymes.[1e,2] In heme iron enzymes, oxoiron(IV) porphyrin π-cation radical (Compound I, Cpd I) and oxoiron(IV) porphyrin (Compound II, Cpd II) species are proposed as reactive intermediates in dioxygen activation and oxygen-atom transfer reactions.[1] Because of its biological significance, the reactivity of Cpd I has been widely investigated with in situ-generated oxoiron(IV) porphyrin π-cation radical complexes in various types of oxidation reactions, such as epoxidations of olefins and hydroxylations of hydrocarbons.[1a,3] The mechanisms of these reactions have been studied experimentally[1e,3c,4] and theoretically.[5] Dissimilar from Cpd I mimics, oxoiron(IV) porphyrins, Cpd II mimics, have been considered to be very poor oxidants[6] and hence have received less attention. However, several instances of experimental evidence have accumulated proving that oxoiron(IV) porphyrin complexes are competent oxidants of a variety of substrates. Groves and co-workers first reported that an oxoiron(IV) porphyrin complex, (TMP)Fe^{IV}=O (TMP = tetramesitylporphyrinate) is able to oxidize olefins.[7] Several years later, Nam and co-workers reported that oxoiron(IV) porphyrins are also able to activate C−H bonds of alkanes, thereby yielding alcohol products.[6a] These authors demonstrated that an oxoiron(IV) porphyrin complex bearing an electron-deficient porphyrin ligand, (TPFPP)Fe^{IV}=O (TPFPP = *meso*-tetrakis(pentafluorophenyl)-porphyrinate), is able to conduct two-electron oxidations of olefins to epoxides and of alkanes to alcohols, with high stereoselectivity and reactivities similar to those found for Cpd I mimics. More recently, experimental studies by Nam, Fukuzumi, and co-workers have shown that oxoiron(IV) porphyrin complexes bearing electron-deficient porphyrin ligands are the active oxidants in the oxidations of alkyl aromatics.[8]

In contrast with this experimental evidence, but in line with the general credence that the hydrogen-atom abstraction ability of Cpd II is much weaker than that of Cpd I,[6] a quantum mechanics/molecular mechanics (QM/MM) study on the relative hydrogen-abstraction capabilities of Cpd I and Cpd II in a P450$_{cam}$ model predicted sluggish oxidative properties for the latter, with H-abstraction barriers of about 5 kcal/mol higher than those computed for Cpd I.[5d] A density functional theory (DFT) study by de Visser, Nam and co-workers[5c] on the AcrH$_2$ (AcrH$_2$ = 10-methyl-9,10-dihydro acridine) hydroxylation by a Cpd I mimic, [(Por$^{+\bullet}$)(Cl)Fe^{IV}=O], and its one-electron reduced form, [(Por)(Cl)Fe^{IV}=O]$^-$, came to similar conclusions. Both these complexes proved to be plausible oxidants with the former showing lower (ca. 4 kcal/mol) H-abstraction barrier than the latter. It was also found that Cpd I, but not Cpd II, is able to react via hydride transfer, a route that proved to be

Received: June 9, 2012
Published: September 4, 2012

   dx.doi.org/10.1021/ic301232r | *Inorg. Chem.* 2012, 51, 9833−9845

much more efficient than the classic hydrogen-abstraction route.[5c]

Theory could be reconciled with experiment if the oxidizing power of Cpd II mimics were related to the electron-deficient character of the porphyrin ligand. This seems not to be the case, however. As a matter of fact, a Cpd II mimic bearing an electron-deficient porphyrin ligand, [(4-TMPyP)Fe^{IV}=O] (4-TMPyP = 5,10,15,20-tetrakis(N-methyl-4-pyridinium) porphyrinate) has been recently found to be almost unreactive toward C−H hydroxylations, whereas its one-electron oxidized form (Cpd I) has proven to be an extremely reactive oxidant in C−H hydroxylation reactions.[9]

Thus, the reactivity of Cpd II seems to be still controversial and a thoroughly and systematic analysis of the electronic factors governing its reactivity is in order.

In this paper we report a detailed DFT electronic structure analysis of alkane hydroxylation by axially unligated and hydrosulfide (HS^-) ligated iron(IV)-oxo porphyrins, $PorFe^{IV}$=O and $[Por(SH)Fe^{IV}=O]^-$ (Por = porphyrinate). Methane was chosen as model for the alkane. While this is a naive choice its results can be used to model trends and to make predictions on relevant data. With these model systems we studied the hydroxylation process in the rebound mechanism originally proposed by Groves and McClusky[10] and generally accepted for the activation of C−H bonds by oxo-iron(IV) compounds (Scheme 1).

Scheme 1. Schematic Representation of the Rebound Mechanism

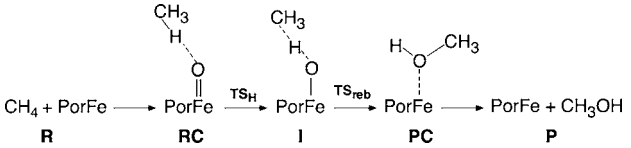

This mechanism involves two steps: (1) hydrogen-atom abstraction from the substrate R−H via transition state $\mathbf{TS_H}$ to form an intermediate complex, **I**, where an iron(III)-hydroxo species is weakly bound to the alkyl radical R·, and (2) alkyl radical rebound on the Fe(III)-hydroxo complex via transition state $\mathbf{TS_{Reb}}$ to generate the alcohol product complex, **PC**, which then releases the hydroxylated product R−OH and restores the iron(II) complex.

The methane hydroxylation reaction was studied on the ground triplet and excited quintet spin-state surfaces. It is well-known that the activation barriers may change significantly depending on the spin multiplicity of the potential energy surfaces, and the reactants may go through more than one such surfaces during the reaction.[5a,11]

Besides the spin multiplicity of the potential energy surface, an important aspect of the alkane hydroxylation reaction concerns the topology of the substrate C−H bond approach. The substrate C−H bond may attack the ferryl unit either vertically or horizontally, depending on the acceptor orbital of the catalyst. A Fe−O σ^* acceptor orbital requires a vertical approach of the cleaving C−H bond (σ-attack), and a Fe−O π^* acceptor orbital requires an equatorial approach (π-attack).[12] On the quintet surface the reaction usually follows a σ-mechanism, whereas on the triplet surface the π-mechanism is the preferred one (for heme systems, see, for instance, refs. 12,13). However, Solomon and co-workers[14] found that in the benzylic hydroxylation of (4-hydroxy)mandelate synthase (HmaS) the H-abstraction step on the quintet surface proceeds through a π-mechanism rather than through the usual σ-mechanism. Furthermore, recent DFT studies by Neese and co-workers[15] of the alkane hydroxylation reaction by nonheme model compounds have shown that a quintet π-pathway is a generally competitive reaction channel and a σ-pathway is also feasible on the triplet surface, as illustrated in Scheme 2.

Scheme 2. Plausible Reaction Channels for the Hydrogen-Atom Abstraction by Oxoiron(IV) Complexes

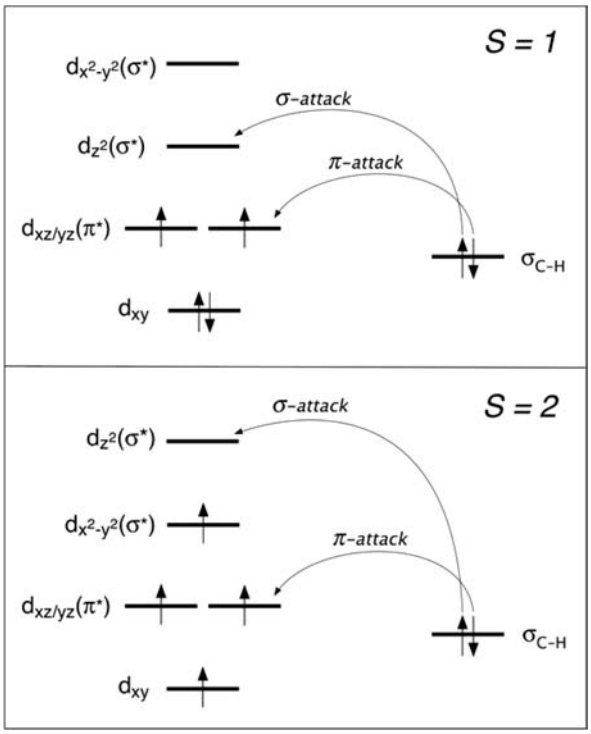

In the light of these findings, for the methane hydroxylation reaction by the Cpd II mimics here considered all four possible channels were explored.

Concerning the C−H bond activation mechanism by oxoiron(IV) species the issue of which is the actual acceptor orbital in the H-abstraction step merits to be addressed.

According to the common view the H-abstraction reaction is an electrophilic attack by the catalyst. In this reaction the σ_{C-H} molecular orbital (MO) of the substrate is the donor orbital and the Fe−O σ^* or one of the Fe−O π^* serve as acceptor MO.[16] The efficiency of the process has been suggested to depend on three electronic factors: (1) the oxygen content of the acceptor orbital (the substrate can only interact with the oxo group rather than directly with the iron center); (2) the energy of the acceptor orbital (there should be a favorable energy match between the donor and acceptor MOs); (3) the overlap between the interacting MOs (a σ-attack is in general more efficient than a π-attack). The role of the Fe−O σ^* and Fe−O π^* as acceptor MOs has been recently debated by Solomon,[14] Neese[15,17] and their co-workers. On the basis of the electronic structure analysis of the transition state of the H-atom abstraction reaction by nonheme oxoiron(IV) species, these authors came to the conclusion that the H-abstraction process should involve a "preparatory step" in which a ferric-oxyl species, Fe(III)−$O^{\bullet-}$, is produced and that the intrinsic electron acceptor in the process is an oxyl-p orbital rather than the Fe−O σ^* or π^*. Also, the localization of an electron hole on the oxo, and the concomitant

dx.doi.org/10.1021/ic301232r | Inorg. Chem. 2012, 51, 9833−9845

$Fe^{IV} \rightarrow Fe^{III}$ reduction was shown to be independent of the substrate and reachable by simply elongating the Fe−O bond.

In this paper the question concerning the nature of the actual acceptor orbital in the H-abstraction step has been specifically addressed. To answer this question a detailed electronic structure analysis of the transition state species as well as of reactant complexes en route to the transition state was performed.

METHODS

All calculations were performed with Turbomole V6.3 2011[18] using the hybrid B3LYP[19] functional in combination with the extensively polarized basis sets of triple-ζ quality including high angular momentum polarization functions (def2-TZVP).[20] Geometry optimizations were performed without constraints. The subsequent frequency calculations verified that all local minima had only real frequencies and that transition states were characterized by a single imaginary frequency. The zero-point energies (ZPE) were obtained from these frequency calculations. The atomic orbital contribution to the MOs has been computed through a Mulliken population analysis using the AOMix program.[21]The effects of the environment on the activation barriers were tested through single point calculations using a dielectric continuum model, which was chosen to be the COSMO[22] model. A dielectric constant of $\varepsilon = 5.7$ and probe radius of 2.7 Å mimicking a chlorobenzene solution were used. These values proved to be in line with values found for enzymatic systems.[23]

RESULTS AND DISCUSSION

Molecular and Electronic Structure of the Oxoiron(IV) Porphyrin Complexes. The key geometrical parameters, relative energies, and Mulliken spin populations computed for $PorFe^{IV}=O$ and $[Por(SH)Fe^{IV}=O]^-$ in the triplet and quintet spin states are reported in Table 1.

Table 1. Bond Lengths (Å), Spin Densities (ζ), and Relative Energies (kcal/mol) of $PorFe^{IV}=O$ and $[Por(SH)Fe^{IV}=O]^-$ in the $S = 1$ and $S = 2$ Spin States

	$PorFe^{IV}=O$		$[Por(SH)Fe^{IV}=O]^-$	
	$S = 1$	$S = 2$	$S = 1$	$S = 2$
Fe−O	1.608	1.621	1.658	1.657
Fe−S			2.487	2.488
Fe−N[a]	2.014	2.090	2.028	2.090
ΔE[b]	0.0	7.3	0.0	7.0
ζ_{Fe}	1.25	3.34	1.22	3.18
ζ_O	0.78	0.45	0.88	0.71
ζ_S			0.00	−0.11
ζ_N	0.00	0.04	0.00	0.01

[a]Average value. [b]Energies include ZPE correction.

According to the calculated energies and in line with the expectation,[3d] both complexes have a triplet ground state, with the quintet lying about 7 kcal/mol higher in energy.

$PorFe^{IV}=O$ and $[Por(SH)Fe^{IV}=O]^-$ in the triplet ground state retain the distinctive electronic structure features of most $S = 1$ iron(IV)-oxo complexes studied so far, as inferred from Figures 1 and 2 where the spin unrestricted energy level diagrams and relevant molecular orbitals of $^{3,5}PorFe^{IV}=O$ and $^{3,5}[Por(SH)Fe^{IV}=O]^-$ are displayed. The $Fe^{IV}=O$ ($S = 1$) moiety is a d^4 system with a $(d_{xy})^2(d_{xz})^1(d_{yz})^1$ electronic configuration. The Fe−O bond is formed by a σ interaction between the (nominally occupied) O-2p_z orbital and the (nominally unoccupied) Fe-d_{z^2} orbital, and a π interaction between the (nominally occupied) O-2$p_{x,y}$ and the (nominally half occupied) Fe-$d_{xz,yz}$ orbitals. Of the Fe-d_δ orbitals, the fully occupied d_{xy} is substantially a nonbonding orbital, whereas the empty $d_{x^2-y^2}$ with lobes along the axes is destabilized by antibonding interaction with the σ lone pairs of the equatorial pyrrolic nitrogens. This MO, denoted hereafter as σ'^*, ends up above the lowest unoccupied porphyrin orbitals, the "e_g*". As can be inferred from the diagrams of Figures 1 and 2 the quintet electronic configuration differs from the triplet configuration by a spin-forbidden single ligand field transition from the β-spin d_{xy} to the α-spin $d_{x^2-y^2}$ (σ'^*). As the latter is strongly Fe−N σ-antibonding, but both are (nearly) perpendicular to the Fe−O bond, the Fe−O bond length does not change significantly in going from the triplet to the quintet state, but the equatorial ligands bind much more strongly to the central iron in the triplet than in the quintet (Table 1). The surplus of α-spin electrons in the quintet creates a strongly stabilizing exchange potential pulling all α-spin levels, including the d_{z^2} (σ^*), very much down compared to the corresponding β-spin levels. The diagrams in Figure 2 show that the introduction of a negatively charged axial ligand destabilizes all levels, particularly the Fe−O σ^* that is subject of an additional destabilization because of the antibonding with the sulfur lone pair (see the plot of this MO in Figure 2).

With regard to reactivity, some electronic structure features of the investigated Cpd II mimics deserve attention. In the first place, the relative energy of the α-spin σ^* and the pair of β-spin π^*, which are the potential acceptor MOs, and the energy match between these orbitals and the methane σ_{C-H} donor MO. In the triplet ground state, the α-spin σ^* and the pair of β-spin π^* have similar energy in the unligated complex, but not in the hydrosulfide-ligated complex, where the former is well above the latter. In the quintet state the large exchange stabilization of the α-spin orbitals lowers the α-spin σ^*, which lies well below the pair of β-spin π^* in both complexes, especially in the unligated one. Whatever the spin state is, the acceptor orbitals of $PorFe^{IV}=O$ and $[Por(SH)Fe^{IV}=O]^-$ are much higher in energy (8−9 eV) than the methane σ_{C-H} orbital, in the actual potential of the reactant complex. Thus, it is unlikely that the approaching substrate interacts directly with the acceptor orbitals of the catalyst, at least not at the early stage of the reaction.

In the second place, the oxygen content of the potential acceptor orbitals is rather low, particularly in the hydrosulfide-ligated complex. The oxygen-rich MOs of the ferryl moiety are, instead, the *occupied* Fe−O π-bonding and especially the Fe−O σ-bonding MOs (cf the O-2p contribution to these MOs in Figures 1 and 2).

Methane Hydroxylation by $PorFe^{IV}=O$. The potential energy profiles for methane hydroxylation by $^{3,5}PorFe^{IV}=O$ are shown in Figure 3. The relevant energy data are summarized in Table 2. Tables 3 and 4 collect the salient geometrical features of the key local minima and transition states computed on the triplet and quintet surfaces, respectively.

According to the calculated activation barriers, the rate-determining step of the hydroxylation reaction is the H-atom transfer from the substrate, both on the triplet and quintet surfaces. The subsequent OH-rebound step involves quite low barriers, with $\Delta E^{\#}_{TS_{Reb}}$ values ranging from 2.0 to 4.4 kcal/mol.

Hydrogen-Atom Abstraction: Energetics and Electronic Structure Analysis. Initially, the two reactive states of $PorFe^{IV}=O$ form reactant complexes, ^{3,5}**RC**, in which $PorFe^{IV}=O$ is weakly bound to methane. On the triplet surface the H-abstraction step can proceed either through the classic π-channel or through the nonclassical σ-channel, with the latter being favored, as indicated by the pertinent $\Delta E^{\#}_{TS_{H\pi}}$ and $\Delta E^{\#}_{TS_{H\sigma}}$ values (Table 2).

dx.doi.org/10.1021/ic301232r | Inorg. Chem. 2012, 51, 9833−9845

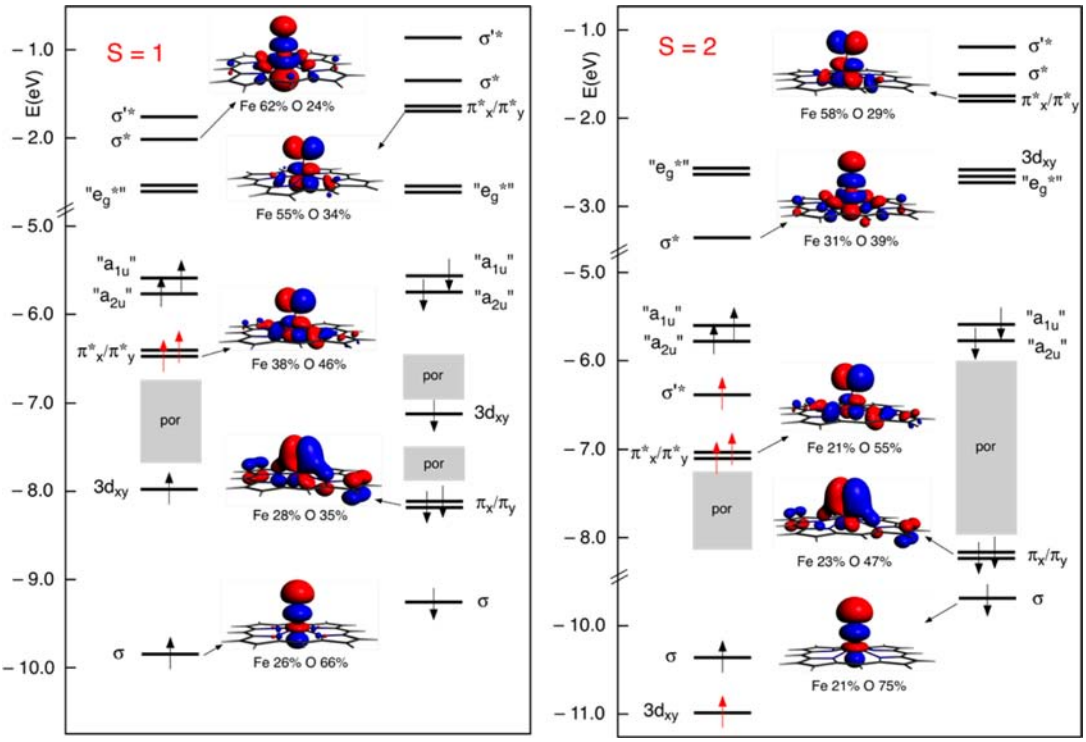

Figure 1. Energy level diagram and relevant molecular orbitals of PorFe^{IV}=O in the triplet (S = 1) and quintet (S = 2) spin states.

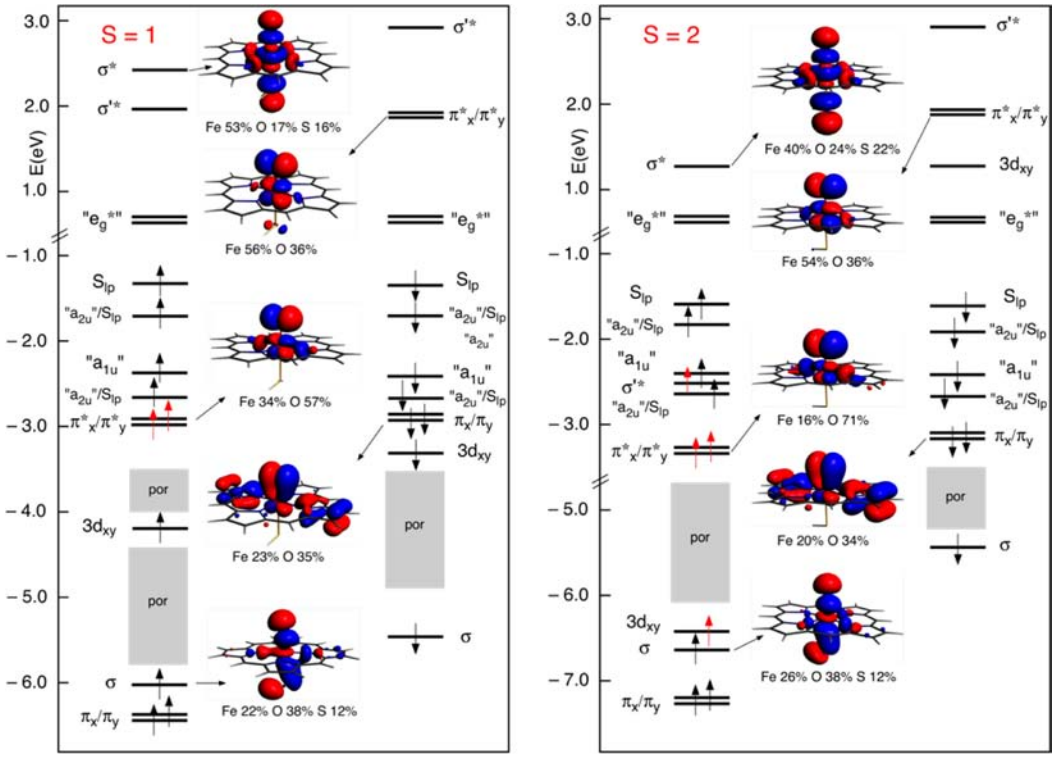

Figure 2. Energy level diagram and relevant molecular orbitals of ^{3,5}[Por(SH)Fe^{IV}=O]$^-$ in the triplet (S = 1) and quintet (S = 2) spin states.

On the quintet surface the H-abstraction barrier could only be located for the classic σ-mechanism.

The $\Delta E^{\#}_{TS_H}$ values reported in Table 2 indicate that the quintet σ-pathway encounters a much lower barrier (11.7 kcal/mol relative to ^{5}**RC**) than the triplet channels. Inclusion of environment effects slightly lowers the barriers by at most 2.2 kcal/mol and does not change the ordering of the transition states so that, either in the gas phase or in a low polarity medium, the quintet surface cuts through the triplet surfaces, thereby providing, in principle, a lower energy path for the reaction. Thus, a two-state reactivity (TSR) mechanism with crossover from the ground state triplet surface to the quintet state surface is a plausible scenario for C−H bond activation by PorFe^{IV}=O. A TSR mechanism has also been envisaged for C−H bond

dx.doi.org/10.1021/ic301232r | Inorg. Chem. 2012, 51, 9833−9845

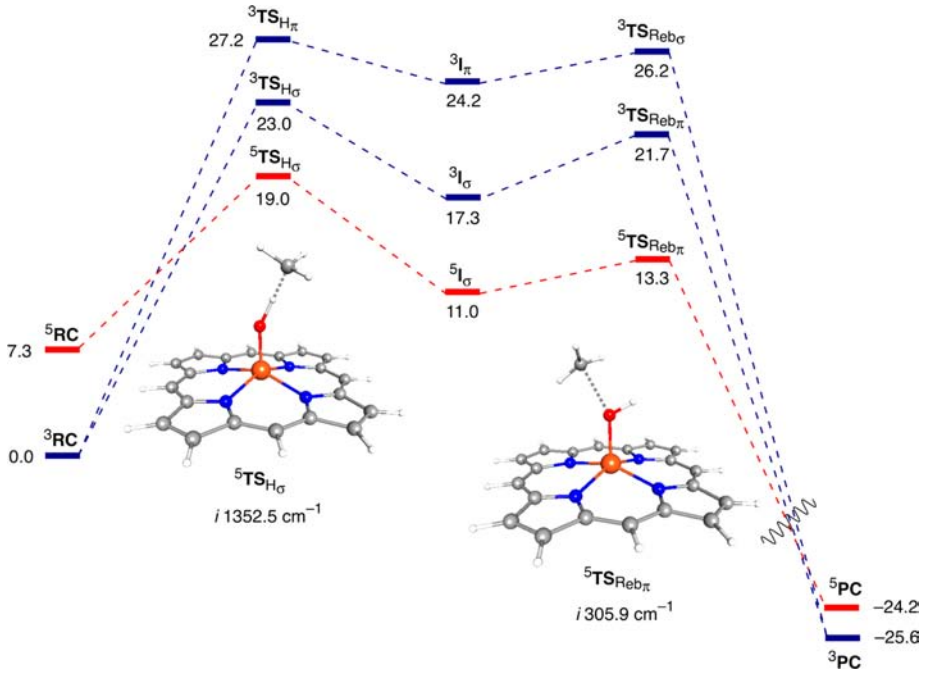

Figure 3. Potential energy profiles for methane hydroxylation by ^{3,5}PorFe^{IV}=O. Energies are in kcal/mol and include ZPE correction. Also shown are the molecular structures of $^5\mathbf{TS}_{\mathbf{H}_\sigma}$ and $^5\mathbf{TS}_{\mathbf{Reb}_\pi}$.

Table 2. Energy Data (kcal/mol) for Methane Hydroxylation by ^{3,5}PorFe^{IV}=O^{a,b}

	$\Delta E^{\#}_{TS_{H\sigma}}$	$\Delta E^{\#}_{TS_{H\pi}}$	ΔE_{I_σ}	ΔE_{I_π}	$\Delta E^{\#}_{TS_{Reb\pi}}$	$\Delta E^{\#}_{TS_{Reb\sigma}}$	ΔE_{PC}
^{3}PorFe^{IV}=O	23.0 (22.8)	27.2 (25.0)	17.3[c]	24.2	4.4 (8.7)	2.0 (5.0)	−25.6
^{5}PorFe^{IV}=O	11.7 (11.4)		3.7		2.3 (4.4)		−31.5

[a]Energy values include ZPE correction; the energy values in parentheses also include the dielectric energy contribution. [b]$\Delta E^{\#}_{TS_H}$= $E(TS_H) - E(RC)$; ΔE_I= $E(I) - E(RC)$; $\Delta E^{\#}_{TS_{Reb}}$= $E(TS_{Reb}) - E(I)$; $\Delta E_{PC} = E(PC) - E(RC)$. [c]The energy value refers to separate iron(III)-hydroxo (S = 3/2) and methyl radical (S = −1/2) species.

Table 3. Bond Lengths (Å) and Bond Angles (deg) of the Key Local Minima and Transition States on the Triplet Surfaces for Methane Hydroxylation by PorFe^{IV}=O

	^{3}RC	$^3TS_{H_\pi}$	$^3TS_{H_\sigma}$	$^3I_\pi$	$^3I_\sigma$[a]	$^3TS_{Reb_\sigma}$	$^3TS_{Reb_\pi}$	^{3}PC
Fe−O	1.609	1.737	1.766	1.782	1.866	1.827	1.907	2.448
Fe−N[b]	2.014	2.013	2.026	2.011	2.028	2.011	2.024	2.011
O−H	2.564	1.105	1.124	0.970	0.963	0.967	0.964	0.964
C−H	1.090	1.452	1.387	2.482				
C−O						2.499	2.337	1.429
∠FeOH	173.4	120.5	149.2	110.5	117.4	109.6	116.5	
∠FeOC						157.8	147.7	123.5
∠OHC	179.4	170.4	174.8	147.8				

[a]The geometrical data refer to the intermediate spin (S = 3/2) iron(III)-hydroxo complex. [b]Average value.

activation by nonheme Fe^{IV}=O complexes.[16f,24] Given the quite large triplet/quintet energy gap (7.3 kcal/mol) between the reactant complexes, the C−H bond activation reaction by PorFe^{IV}=O is expected to start on the triplet surface and cross over the quintet state en route to the transition state, with a probability that depends on the spin−orbit coupling (SOC) interaction between the two spin states.[25] As the initial spin-states energy gap is quite large, the crossing is expected to occur at an advanced stage of the reaction, namely, when the SOC value is significantly reduced relative to the initial stage because of the delocalization of the orbitals of the two states. This means that there is a high probability of staying on the triplet state and the net barrier for the H-abstraction reaction is a blend of the triplet and quintet barriers, the triplet contribution being dominant.[16f]

Consistent with the H-abstraction barriers computed for the triplet σ- and π-pathways, $^3\mathbf{TS}_{\mathbf{H}_\sigma}$ shows shorter C−H bond and longer O−H bond than $^3\mathbf{TS}_{\mathbf{H}_\pi}$ (Table 3). In turn, $^5\mathbf{TS}_{\mathbf{H}_\sigma}$ shows C−H and O−H bond distances that fit in with this species occurring earlier than the $^3\mathbf{TS}_{\mathbf{H}}$ species. The Fe−O−H angle, which is a distinctive geometrical feature of the $\mathbf{TS}_{\mathbf{H}}$ species as it reflects the type of attack (vertical or horizontal) of the cleaving C−H bond to the ferryl unit, is 149.2°, 120.5°, and 149.7° in $^3\mathbf{TS}_{\mathbf{H}_\sigma}$, $^3\mathbf{TS}_{\mathbf{H}_\pi}$, and $^5\mathbf{TS}_{\mathbf{H}_\sigma}$, respectively. All $\mathbf{TS}_{\mathbf{H}}$ structures

dx.doi.org/10.1021/ic301232r | Inorg. Chem. 2012, 51, 9833−9845

Table 4. Bond Lengths (Å) and Bond Angles (deg) of the Key Local Minima and Transition States on the Quintet Surface for Methane Hydroxylation by $PorFe^{IV}$=O

	^{5}RC	$^5TS_{H_\sigma}$	$^5I_\sigma$	$^5TS_{Reb_\pi}$	^{5}PC
Fe−O	1.623	1.746	1.825	1.872	2.252
Fe−N[a]	2.090	2.102	2.106	2.101	2.081
O−H	2.499	1.191	0.968	0.963	0.964
C−H	1.090	1.301	2.332		
C−O				2.301	1.433
∠FeOH	180.0	149.7	123.8	119.5	
∠FeOC				136.6	125.2
∠OHC	180.0	177.9	170.3		

[a]Average value.

involve a nearly collinear O−H−C moiety, which is typical of H-abstraction processes.

The salient electronic structure features of the TS_H species are illustrated in Figures 4−6. The schematic MO diagram of $^3TS_{H_\sigma}$

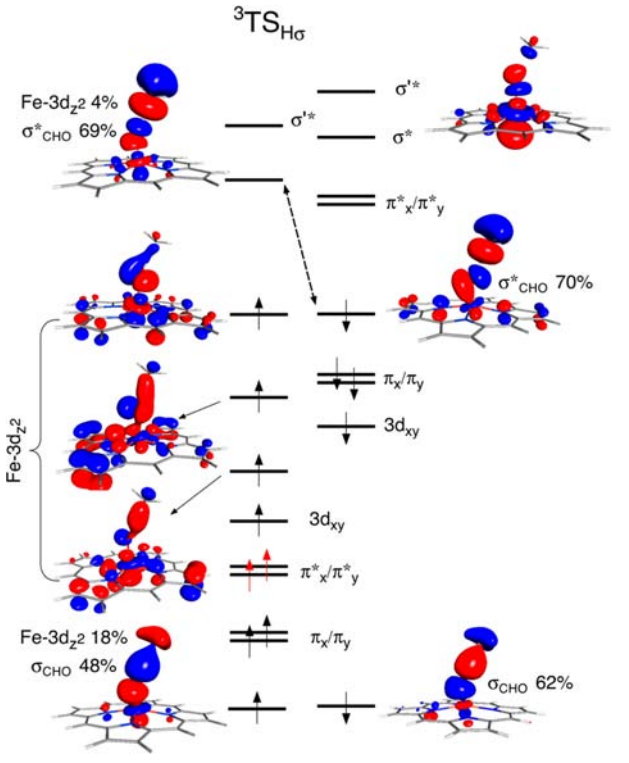

Figure 4. Schematic MO diagram for $^3TS_{H_\sigma}$.

(Figure 4) shows that significant electronic structure changes occur upon approaching the transition state.

In the spin-up manifold the Fe−O σ^* has lost most of the original $3d_{z^2}/4p_z$ hybrid character becoming basically a three-centered σ_{C-H}/O-2p_z σ-antibonding MO, hereafter denoted as σ^*_{CHO}. The $3d_{z^2}/4p_z$ hybrid character of the original α-spin σ^* has moved to a set of (three) lower-lying occupied MOs. Thus, three of the five Fe-3d orbitals, the $3d_\pi$ and $3d_{z^2}$, are formally singly occupied. The MO diagram of Figure 4 also shows that the low-lying α-spin and β-spin Fe−O σ-bonding orbitals are engaged in a σ-bonding interaction with the methane σ_{C-H} orbital and are best described as three-centered σ_{CHO} orbitals. Notably, in the spin-down manifold there is a high-lying, singly

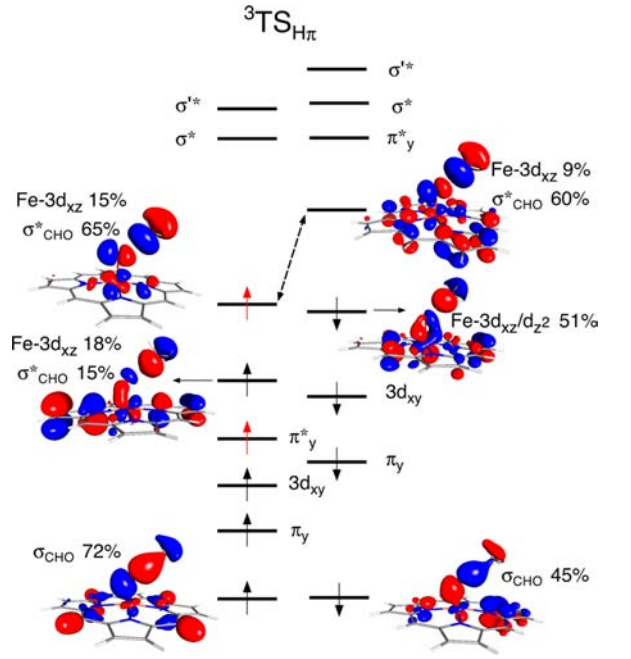

Figure 5. Schematic MO diagram for $^3TS_{H_\pi}$.

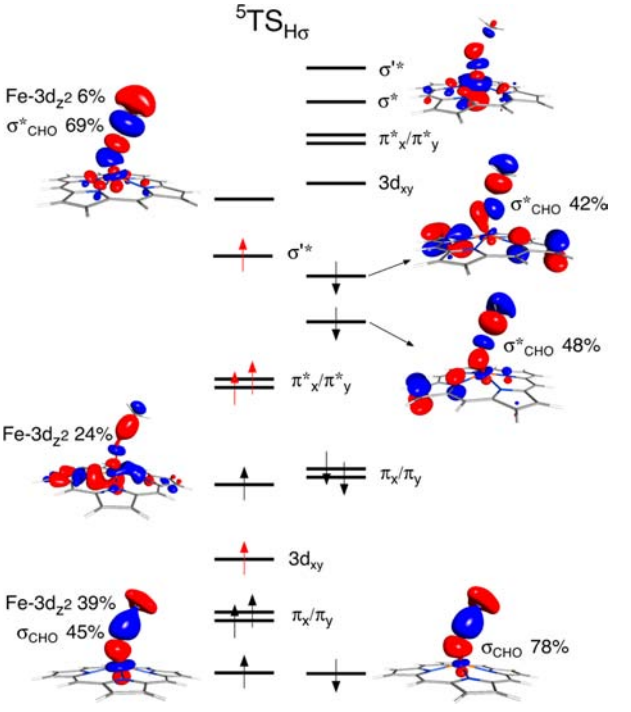

Figure 6. Schematic MO diagram for $^5TS_{H_\sigma}$.

occupied molecular orbital (SOMO), that is largely a σ^*_{CHO} MO. By virtue of its Fe−O σ-bonding character, this MO can be conceived as the antibonding counterpart of the low-lying β-spin σ_{CHO}.

The orbital occupation pattern of $^3TS_{H_\sigma}$ configures a situation in which an intermediate spin Fe(III) center (S = 3/2) is "antiferromagnetically" coupled to a three-center C−H−O radical (S = 1/2).

The H-abstraction process on the triplet surface through a σ-mechanism does not lead to a stable intermediate, rather the

dx.doi.org/10.1021/ic301232r | Inorg. Chem. 2012, 51, 9833−9845

system evolves toward an intermediate spin iron(III)-hydroxo complex (S = 3/2) and a methyl radical (S = −1/2), thus preserving the overall triplet state.

According to the MO diagram of ^{3}**TS**$_{H_\pi}$ in Figure 5, the major electronic structure changes occurring upon approaching the transition state involve the spin-up and spin-down Fe−O π_X* MOs, which lose most of the original Fe-3d$_{xz}$ character and become largely σ^*_{CHO} orbitals. The Fe-3d$_{xz}$ character shifts to lower lying occupied MOs (see for instance the plot of the highest β-spin singly occupied MO (SOMO) in the diagram of Figure 5) to the result that the Fe-3d$_{xz}$ orbital gets fully occupied. The occupation pattern of ^{3}**TS**$_{H_\pi}$ is consistent with a low-spin Fe(III) center (S = 1/2) "ferromagnetically" coupled to a three-center C−H−O radical (S = 1/2). It is worth noting that ^{3}**TS**$_{H_\pi}$, just as ^{3}**TS**$_{H_\sigma}$, features low-lying α- and β-spin σ_{CHO} MOs. These are generated by a bonding interaction between the Fe−O σ and, to some extent, Fe−O π_X MOs of the catalyst and the methane σ_{C-H} orbital.

After passing ^{3}**TS**$_{H_\pi}$, the singly occupied σ^*_{CHO} MO evolves to the methyl carbon radical, whereas the low-lying α- and β-spin σ_{CHO} MOs convert to the σ-bonding orbital of the O−H group. The resulting intermediate, ^{3}**I**$_\pi$, is a low-spin iron(III)-hydroxo complex (S = 1/2) "ferromagnetically" coupled to a methyl radical (S = 1/2).

The main electronic structure changes occurring upon approaching ^{5}**TS**$_{H_\sigma}$ involve the same orbitals as seen in ^{3}**TS**$_{H_\sigma}$. According to the MO diagram of Figure 6, the α-spin σ* loses most of the 3d$_{z^2}$/4p$_z$ hybrid character and becomes a σ^*_{CHO} MO. The 3d$_{z^2}$/4p$_z$ hybrid character of the original α-spin σ* moves into lower lying occupied MOs. In turn, both components of the Fe−O σ-bonding MO are engaged in a bonding interaction with the methane σ_{C-H} orbital becoming, especially the β-spin component, largely σ_{CHO} orbitals. The antibonding counterpart of the β-spin σ_{CHO} splits into close-lying MOs, the two highest SOMOs in the diagram of Figure 6. The orbital occupation pattern of ^{5}**TS**$_{H_\sigma}$ configures a high-spin (S = 5/2) Fe(III) (five occupied α-spin Fe-3d orbitals, no occupied β-spin Fe-3d orbitals) center leading to the Fe(III)-hydroxo intermediate, ^{5}**I**$_\sigma$, with a high-spin (S = 5/2) on the iron, "antiferromagnetically" coupled to the methyl radical (S = 1/2), maintaining the total spin S = 2.

Of the three intermediates, ^{5}**I**$_\sigma$ is by far the most stable one, which is consistent with Fe(III)-hydroxo porphyrins having a high-spin (S = 5/2) ground state.[26]

Hydrogen-Atom Abstraction: The Nature of the Acceptor Orbital. An important point to arise from the electronic structure of the **TS**$_H$ species is that the H-abstraction process involves, besides the α-spin σ* and β-spin π* acceptor orbitals of the catalyst, the low-lying, oxygen-rich, Fe−O σ- and/or π-bonding MOs. This implies that this process is rather complex and cannot be simply described in terms of a *direct* electron transfer from the σ_{CH} of the substrate to the α-spin σ* or β-spin π* acceptor orbital of the catalyst. On the other hand, the salient electronic structure features of the **TS**$_H$ species can hardly be rationalized in terms of formation of a ferric-oxyl species, as proposed by Neese et al.[17,27] and by Solomon et al.,[14] for the case of alkane H-abstraction reactions by nonheme oxoiron(IV) complexes. As a matter of fact, we do not have evidence supporting the formation of a ferric-oxyl species during the reaction. For instance, the "empty" α-spin σ^*_{CHO} orbital has in ^{3}**TS**$_{H_\sigma}$ and ^{5}**TS**$_{H_\sigma}$approximately the same oxygen content as in the original ^{3,5}**RC** α-spin Fe−O σ*. Similarly, the "empty" β-spin σ^*_{CHO} orbital has in ^{3}**TS**$_{H_\pi}$ nearly the same oxygen content as in the ^{3}**RC** β-spin Fe−O π*.

To get more insight into the electron transfer process accompanying the H-abstraction reaction, we have then performed a detailed electronic structure analysis of the reactant complexes en route to the transition state, through a relaxed surface scan at a series of fixed values of the reaction coordinate, the O−H distance.

We first examine the triplet σ-pathway. Figure 7 displays a schematic MO diagram of the reactant complex at an intermediate stage of the reaction (O−H = 1.500 Å) and in proximity of the transition state (O−H = 1.250 Å). Only the MOs that are involved in the interaction between the catalyst and the substrate are reported in the diagram. It is apparent from the MO diagram of Figure 7 that at the O−H distance of 1.500 Å the methane σ_{CH} orbital interacts with the α- and β-spin components of the Fe−O σ-bonding and not, as expected, with the α-spin Fe−O σ* MO. This *two-orbital four-electron* interaction generates the σ+σ_{CH} and σ−σ_{CH} bonding and antibonding pair of MOs, the σ_{CH} contribution being dominant in the latter. The σ_{CH}/σ interaction is not inconceivable in view of the high oxygen content of the σ orbital (Figure 1) and the favorable energy match between the interacting MOs (the energy of the σ_{CH} is about −10 eV in the potential of the reactant complex). Notably, the σ_{CH}/σ interaction is already operative in ^{3}**RC**, when the O−H distance is 2.564 Å (Table 3).

A careful analysis of the composition of the key MOs reveals that, at the O−H distance of 1.500 Å, the α-spin σ−σ_{CH} orbital has acquired some of the 3d$_{z^2}$/4p$_z$ hybrid character of the Fe−O σ*, as apparent from the shrunken top lobe and swollen bottom lobe of the 3d$_{z^2}$ in the former. In turn, the Fe−O σ* has acquired some σ_{CH}/O-2p$_z$ antibonding character of the σ−σ_{CH}. This provides a clue for the occupied/virtual σ−σ_{CH}/σ* mixing. No significant σ−σ_{CH}/σ* mixing occurs, instead, in the spin down manifold, on account of the β-spin σ* lying too high in energy to come into play. The σ−σ_{CH}/σ* mixing occurring in the spin up manifold initiates a charge transfer from the occupied σ−σ_{CH} into the empty Fe−O σ*. This charge transfer leads to the *concomitant* elongation of the Fe−O and C−H bonds relative to the ^{3}**RC** species (1.621 vs 1.609 Å and 1.127 vs 1.092 Å, respectively).

As soon as the substrate approaches closer to the catalyst (O−H = 1.125 Å), the σ_{CH}/σ interaction strenghtens and the α-spin and β-spin components of the σ−σ_{CH} rise in energy. This makes the σ−σ_{CH}/σ* mixing occurring in the spin up manifold more effective and enhances the occupied to virtual electron transfer thus inducing further elongation of the Fe−O and C−H bonds. In the spin down manifold the Fe−O σ* is still too high in energy to come into play and the β-spin component of the σ−σ_{CH} remains essentially a three-center σ^*_{CHO} orbital.

At the transition state the MOs depicted in the diagrams of Figure 7 undergo further mixing with the occupied O-2p$_x$-based MOs. This causes the highest α-spin SOMO of Figure 7 to split in the three MOs with sizable 3d$_{z^2}$/4p$_z$ hybrid character displayed in the diagram of Figure 4. The involvement of the O-2p$_x$-based MOs, which is also apparent in the plots of the α-spin and β-spin σ^*_{CHO}, is consistent with the deviation from linearity of the Fe−O−H angle.

As can be inferred from the MO diagrams of Figure 8, the just discussed electron transfer mechanism holds true for the quintet σ-pathway. However, on the quintet surface the σ−σ_{CH}/σ*

dx.doi.org/10.1021/ic301232r | Inorg. Chem. 2012, 51, 9833−9845

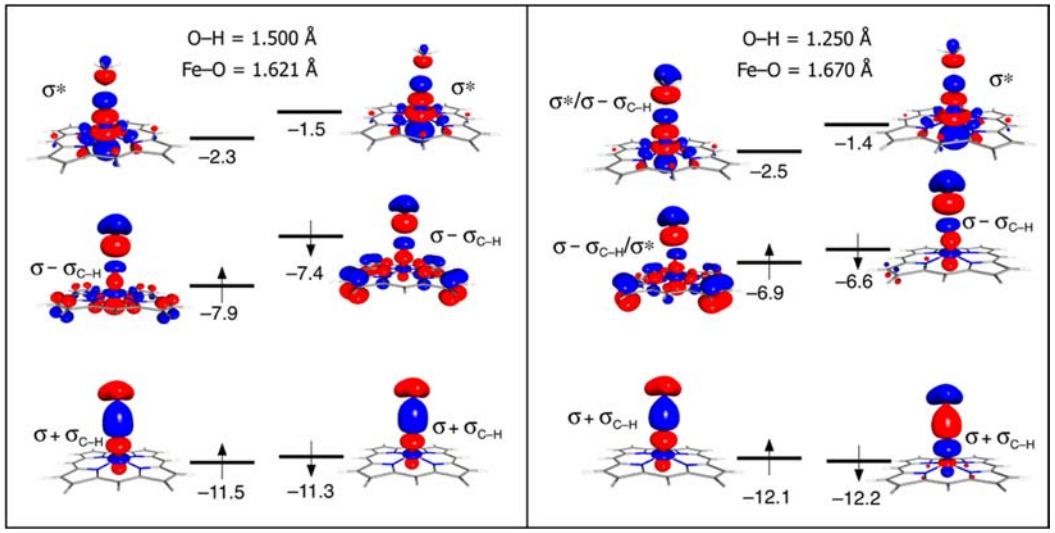

Figure 7. Schematic MO diagram illustrating the evolution of the key MOs of ^{3}**RC** en route to ^{3}**TS**$_{H_\sigma}$. Energies in eV.

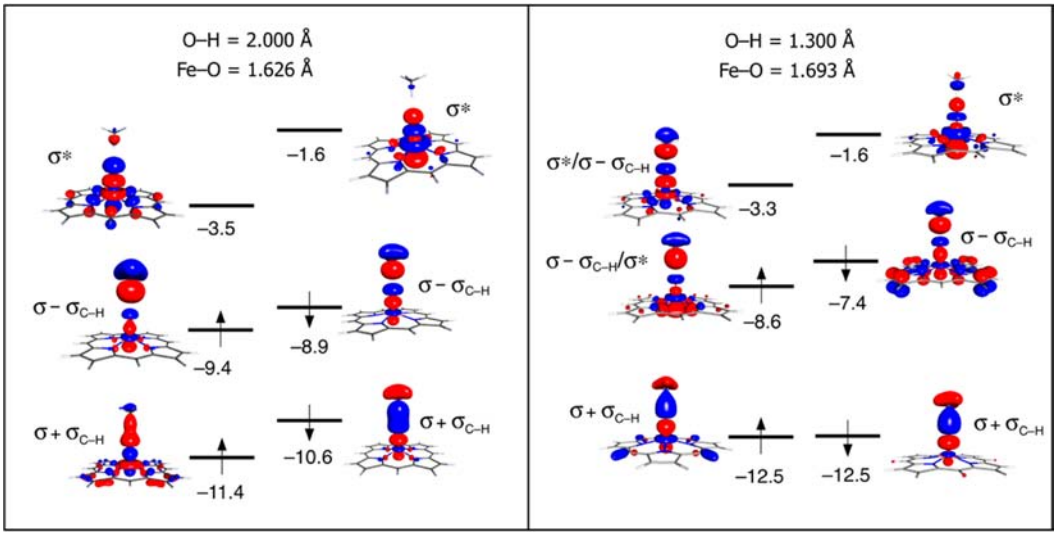

Figure 8. Schematic MO diagram illustrating the evolution of the key MOs of ^{5}**RC** en route to ^{5}**TS**$_{H_\sigma}$. Energies in eV.

mixing occurs at longer O−H distances than on the triplet surface, because of the downward shift of the α-spin σ^* (Figure 1). This explains why ^{5}**TS**$_{H_\sigma}$ is reached earlier and has a lower barrier than ^{3}**TS**$_{H_\sigma}$.

On the triplet π-patway the σ_{CH} orbital of the substrate interacts, initially, with both the Fe−O σ-bonding and the Fe−O π-bonding orbitals of the catalyst. On approaching the transition state the resulting $(\sigma, \pi)-\sigma_{CH}$ antibonding combination mixes with the Fe−O π_X*. In the spin down manifold the Fe−O π_X* is empty to begin with and can accept electron charge from the $(\sigma, \pi)-\sigma_{CH}$. Owing to this occupied/virtual orbital mixing the β-spin Fe−O π_X* progressively looses its $3d_{xz}$ character and becomes eventually a σ^*_{CHO} MO.

In summary, the electronic structure analysis of the **TS**$_H$ species and of the reactant complexes en route to the transition state indicates that the H-abstraction process on the triplet and quintet σ-pathway involves, basically, three key MOs, the σ and σ^* of the catalyst and the σ_{CH} of the substrate. In this process the acceptor orbital is the α-spin Fe−O σ^* while the actual donor orbital is the α-spin $\sigma-\sigma_{CH}$, which is largely a σ_{CH} orbital. On the triplet π-pathway the acceptor orbital is the β-spin Fe−O π_X* and the actual donor MO is the spin down component of the $(\sigma, \pi)-\sigma_{CH}$.

According to the described donor/acceptor interaction scheme, it is clear that there are two main electronic factors controlling the efficiency of the H-abstraction process: (1) the energy match between the substrate σ_{CH} and the Fe−O σ-bonding and/or Fe−O π-bonding orbitals of the catalyst; (2) the energy of the acceptor orbital of the catalyst. The lower is the energy of this orbital, the earlier the mixing with the actual donor orbital occurs.

Rebound Step: Electronic Structure Changes and Electron Transfer Pathways. In the OH rebound step the second electron of the methane σ_{CH} orbital is transferred to an empty Fe−O σ^* or π^* MO of the Fe(III)-hydroxo complex. Depending on the nature of the actual acceptor orbital, the rebound process can proceed through a σ- or a π-pathway. In turn, the nature of the acceptor orbital depends on the type of pathway followed by the H-abstraction process. As pointed out by Neese et al.,[17] a σ-pathway for the H-abstraction is generally followed by a π-channel for the OH rebound step, and a

dx.doi.org/10.1021/ic301232r | Inorg. Chem. 2012, 51, 9833−9845

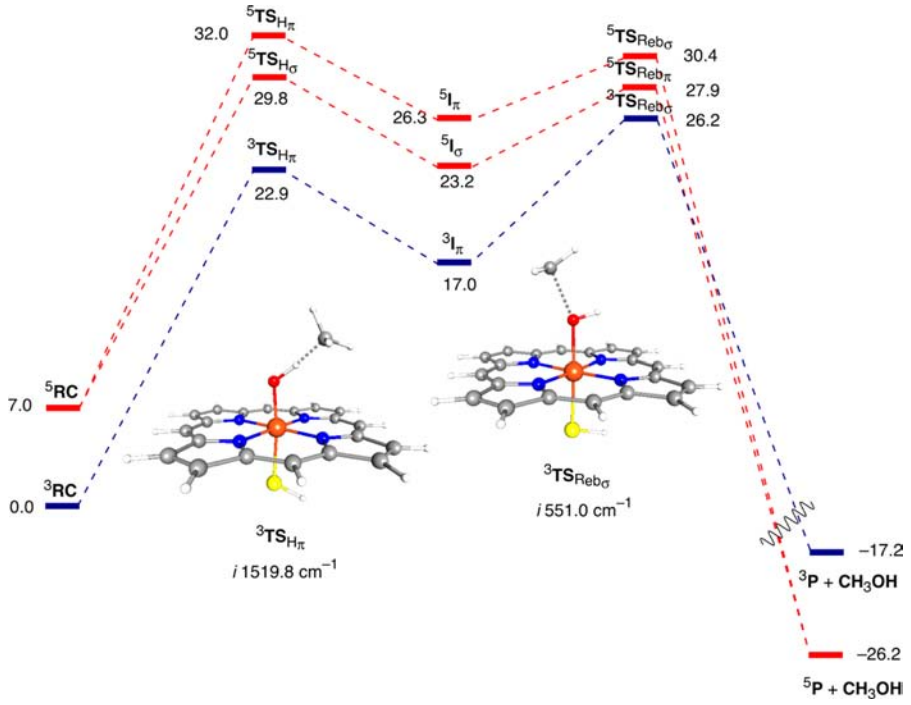

Figure 9. Potential energy profiles for methane hydroxylation by ^{3,5}[Por(SH)Fe^{IV}=O]$^-$. Energies are in kcal/mol and include ZPE correction. Also shown are the molecular structures of ^{3}**TS**$_{H_\pi}$ and ^{3}**TS**$_{Reb_\sigma}$.

π-pathway for the H-abstraction is followed by a σ-channel for the rebound step. The geometrical marker that serves to discriminate between the rebound pathways is the Fe−O−C angle, just as the Fe−O−H angle does in the H-abstraction process.

Starting from ^{3}**I**$_\pi$ the OH rebound step follows a σ-mechanism through ^{3}**TS**$_{Reb_\sigma}$. The remaining α-electron of the methyl radical is transferred into the α-spin σ*. Consistent with the nature of the actual acceptor orbital, in the transition state the methyl radical adopts a nearly vertical orientation, as indicated by the Fe−O−C angle (157.8°), and the Fe−O bond elongates relative to the intermediate ^{3}**I**$_\pi$ (1.827 Å vs 1.782 Å). ^{3}**TS**$_{Reb_\sigma}$ is located quite early on the triplet σ-channel (C−O = 2.499 Å), in agreement with the very low rebound barrier ($\Delta E^{\#}_{TS_{Reb\sigma}}$ = 2.0 kcal/mol).

Starting from ^{3}**I**$_\sigma$ and ^{5}**I**$_\sigma$ the OH rebound step follows a π-mechanism through ^{3}**TS**$_{Reb_\pi}$ and ^{5}**TS**$_{Reb_\pi}$, respectively. In either case the remaining β-electron of the methyl radical is transferred to one of the weakly Fe−O antibonding β−π* MOs and, accordingly, the relative orientation of the methyl radical with respect to the Fe(III)-hydroxo complex is in ^{3}**TS**$_{Reb_\pi}$ and ^{5}**TS**$_{Reb_\pi}$ different from that in ^{3}**TS**$_{Reb_\sigma}$, as indicated by the values of the Fe−O−C angle reported in Tables 3 and 4. We note, in passing, that in ^{3}**TS**$_{Reb_\pi}$ the Fe−O bond is longer and the Fe−O−C angle is larger than in ^{5}**TS**$_{Reb_\pi}$ suggesting that in the former the electron transfer also involves to some extent the strongly Fe−O antibonding β-spin σ* orbital. Both transition states occur later and show a slightly larger barrier than ^{3}**TS**$_{Reb_\sigma}$. ^{3}**TS**$_{Reb_\sigma}$ and ^{3}**TS**$_{Reb_\pi}$ evolve toward the alcohol product complex ^{3}**PC**, in which a low-spin (S = 1) iron(II)porphyrin is very weakly bound to the methanol, as indicated by the rather long Fe−O bond (2.448 Å) and the facile release of methanol (1.9 kcal/mol). In turn, ^{3}**TS**$_{Reb_\pi}$ decays to the alcohol product complex ^{5}**PC**, in which the alcohol is weakly bound to a high-spin (S = 2) iron(II)porphyrin. In the high-spin product complex the interaction between the methanol and the iron(II)porphyrin is, however, not as weak as in ^{3}**PC**, as indicated by the significantly shorter Fe−O bond (2.252 vs 2.448 Å) and the increased dissociation energy (4.9 vs 1.9 kcal/mol).

The actual Fe−O bond length in the product complexes is dictated by the necessity to minimize the steric hindrance between the methanol and the π-system of the macrocycle while preserving an effective Fe−O interaction. In ^{3}**PC**, where the iron atom resides in the porphyrin plane, the Fe−O bond significantly elongates to relieve the steric hindrance between the methanol and the porphyrin π-system. In ^{5}**PC**, where the iron atom lies above the porphyrin plane, because of occupation of the strongly Fe−N σ-antibonding orbital, the steric hindrance between the methanol and the porphyrin π-system is significantly relieved and the Fe−O bond is shorter than in ^{3}**PC**.

In concluding this Section, we note that inclusion of solvation effects raises the rebound barriers by 2.1−4.3 kcal/mol (see Table 2). This is because solvation favors energetically the intermediate relative to the rebound transition state because of a larger solvent exposure of the former. The rise of the rebound barriers, however, does not change the ordering of the transition states, and the H-abstraction step remains the rate-determining step.

Methane Hydroxylation by [Por(SH)Fe^{IV}=O]$^-$: Effects of the Axial Ligand. The potential energy profiles for methane hydroxylation by ^{3,5}[Por(SH)Fe^{IV}=O]$^-$ are shown in Figure 9. The calculated activation barriers, which are reported in Table 5 together with the other relevant energy data computed for the reaction, indicate that also in the case of the hydrosulfide-ligated complex the rate-determining step is the H-abstraction, both on the triplet and quintet surfaces. The reactant complexes formed initially by the triplet and quintet reactive states of [Por(SH)-Fe^{IV}=O]$^-$ are separated by a quite large energy gap (7.0 kcal/mol); thus, the reaction can only start on the lowest energy triplet

dx.doi.org/10.1021/ic301232r | Inorg. Chem. 2012, 51, 9833−9845

Table 5. Energy Data (kcal/mol)[a] for Methane Hydroxylation by ^{3,5}[Por(SH)Fe^{IV}=O]$^-$[a,b]

	$\Delta E^{\#}_{TS_{H\sigma}}$	$\Delta E^{\#}_{TS_{H\pi}}$	ΔE_{I_σ}	ΔE_{I_π}	$\Delta E^{\#}_{TS_{Reb\pi}}$	$\Delta E^{\#}_{TS_{Reb\sigma}}$	ΔE_p
^{3}[Por(SH)Fe^{IV}=O]$^-$		22.9 (19.9)		17.0		9.2 (13.7)	−17.2
^{5}[Por(SH)Fe^{IV}=O]$^-$	22.8 (19.4)	25.0 (21.5)	16.2	19.3	4.7 (9.5)	4.1 (8.5)	−33.2

[a]Energy values include ZPE correction; the energy values in parentheses also include the dielectric energy contribution. [b]$\Delta E^{\#}_{TS_H} = E(TS_H) - E(RC)$; $\Delta E_I = E(I) - E(RC)$; $\Delta E^{\#}_{TS_{Reb}} = E(TS_{Reb}) - E(I)$; $\Delta E_p = E(P) - E(RC)$.

surface. On this surface the H-abstraction barrier could only be located for the classic π-mechanism, most likely because the Fe−O σ* is too high in energy to make a σ-attack of the substrate favorable. As inferred from the MO diagram of ^{3}[Por(SH)-Fe^{IV}=O]$^-$ in Figure 2, the α-spin σ* is, indeed, significantly destabilized by antibonding with the hydrosulfide ligand and lies well above the empty β-spin Fe−O π* MOs. On the triplet π-channel the H-abstraction is found to proceed with a barrier of 22.9 kcal/mol. Only a slightly smaller barrier (20.6 kcal/mol) was predicted by QM/MM calculations for propane H-abstraction by ^{3}[Por(SH)Fe^{IV}=O]$^-$.[5d] In making this comparison one should, however, take into account that different basis sets and computational procedures have been employed in the calculations. Comparing the $\Delta E^{\#}_{TS_{H\pi}}$ values computed for the hydrosulfide-ligated and the unligated complexes (22.9 vs 27.2 kcal/mol), it is apparent that on the triplet π-pathway the former is more reactive than the latter. This holds true also when environment effects are considered (compare the pertinent data in Tables 2 and 5).

We note that the $\Delta E^{\#}_{TS_{H\pi}}$ value computed for the hydrosulfide-ligated Cpd II model system on its ground state triplet surface is slightly lower than the methane H-abstraction barriers computed for ^{2,4}Cpd I.[28] As noted above, however, this comparison may not be fully legitimate.

The H-abstraction barrier lowers on going from the unligated to the hydrosulfide-ligated complex because in the latter the transition state is stabilized by the shortening of the Fe−S bond, as indicated by the pertinent geometrical data of ^{3}**TS**$_{H_\pi}$ in Table 6.

Table 6. Bond Lengths (Å) and Bond Angles (deg) of the Key Local Minima and Transition States on the Triplet Surface for Methane Hydroxylation by [Por(SH)Fe^{IV}=O]$^-$

	^{3}**RC**	^{3}**TS**$_{H_\pi}$	^{3}**I**$_\pi$	^{3}**TS**$_{Reb_\sigma}$	^{3}[Por(SH)Fe]$^-$
Fe−O	1.659	1.806	1.869	1.984	
Fe−S	2.480	2.385	2.363	2.412	2.446
Fe−N[a]	2.028	2.027	2.030	2.028	2.028
O−H	2.385	1.118	0.965	0.965	
C−H	1.091	1.426	2.659		
C−O				2.070	
∠FeOH	163.7	118.7	108.3	106.4	
∠FeOC				156.7	
∠OHC	179.4	174.3	152.9		

[a]Average value.

In other words, the energy penalty associated to the lengthening of the Fe−O bond is mitigated by the energy gain associated to the strenghtening of the Fe−S bond. The same geometrical changes, namely, lengthening of the Fe−O bond and shorthening of the Fe−S bond were found to occur also at the transition state of the methane H-abstraction reaction by ^{2,4}Cpd I.[28]

The presence of the axial hydrosulfide ligand has a negligible impact on the salient electronic structure features of the transition state.

^{3}**TS**$_{H_\pi}$ features, just as in the case of the unligated complex, an occupation pattern that is consistent with a low-spin Fe(III) center (S = 1/2) "ferromagnetically" coupled to a three-center C−H−O radical (S = 1/2) (compare the schematic MO diagrams of Figure 10 and Figure 5). As expected, the electronic

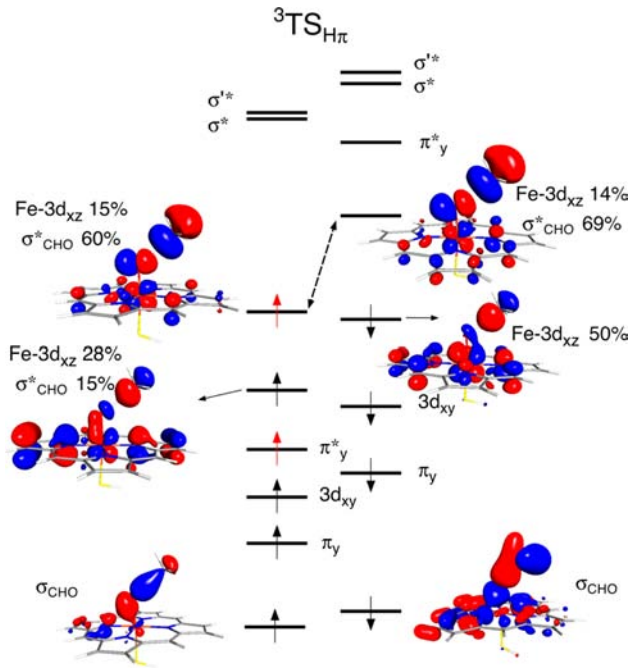

Figure 10. Schematic MO diagram for ^{3}**TS**$_{H_\pi}$.

structure analysis of the reactant complex en route to the transition state reveals that the axial ligand does not modify the electron transfer mechanism described above for the unligated complex. ^{3}**TS**$_{H_\pi}$relaxes to the intermediate ^{3}**I**$_\pi$, which is a low-spin iron(III)-hydroxo complex (S = 1/2) "ferromagnetically" coupled to a methyl radical (S = 1/2).

Starting from ^{3}**I**$_\pi$ the OH rebound step follows a σ-mechanism through ^{3}**TS**$_{Reb_\sigma}$. As the α-electron of the methyl radical is transferred to the α-spin σ*, in the transition state the methyl radical adopts a nearly vertical orientation, the Fe−O−C angle being 156.7° (Table 6). The transition state is located quite late on the triplet σ-channel (C−O = 2.070 Å), in agreement with a relatively high rebound barrier ($\Delta E^{\#}_{TS_{Reb\sigma}}$ = 9.2 kcal/mol). Actually, this barrier is much higher than that computed for the unligated complex on the triplet σ-channel (9.2 vs 2.0 kcal/mol), which is consistent with the α-spin σ* acceptor orbital lying in ^{3}[Por(SH)Fe^{IV}=O]$^-$ at much higher an energy than in ^{3}Por-Fe^{IV}=O. The rebound transition state evolves toward the final reaction products, the methanol and the low-spin (S = 1) pentacoordinate Fe(II) hydrosulfide porphyrin derivative, ^{3}[Por(SH)Fe]$^-$, without forming a stable product complex.

dx.doi.org/10.1021/ic301232r | Inorg. Chem. 2012, 51, 9833−9845

The Fe−O bond breaks and the methanol is released as soon as the C−O distance becomes shorter than 2.00 Å. At this stage the iron atom moves below the N_4 plane to minimize the steric hindrance between the sulfur lone pairs and the π-system of the macrocycle while preserving an effective Fe−S interaction. As a matter of fact, in ^{3}[Por(SH)Fe]$^-$ the iron atom displacement out of the four-nitrogen plane (ΔN_4) is 0.258 Å and the Fe−S distance is 2.446 Å (Figure 11).

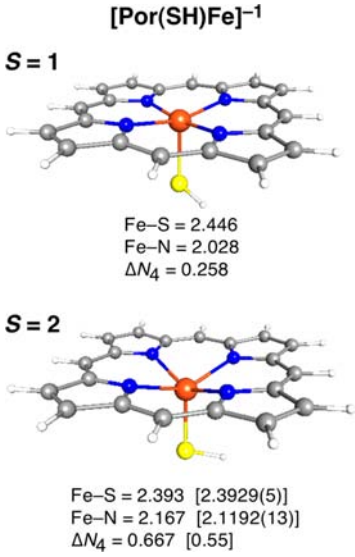

Figure 11. Molecular structure of Fe(II) hydrosulfide porphyrin derivatives in the $S = 1$ and $S = 2$ spin states. Distances are given in Å. Experimental data for [OEP(HS)Fe]$^-$ from ref 29 in square brackets.

On the quintet surface the H-abstraction reaction can proceed either through the classic σ-channel or the nonclassical π-channel, with the former being slightly favored, as indicated by the $\Delta E^{\#}_{TS_{H\sigma}}$ and $\Delta E^{\#}_{TS_{H\pi}}$ values in Table 5. As the quintet surface lies above the triplet surface in the entrance channel of the oxidative process and is highly destabilized on both the σ-and π-pathways during the process, a TSR mechanism with crossover from the ground state triplet surface to the quintet state surface is not a plausible scenario for C−H bond activation by [Por(SH)-Fe^{IV}=O]$^-$. This picture is not altered upon inclusion of environment effects (see Table 5), because these only consist in a modest and nearly uniform lowering (3.0−3.5 kcal/mol) of the transition state barriers. The occupation pattern of ^{5}**TS**$_{H_\sigma}$ is coherent with a high-spin ($S = 5/2$) Fe(III) center "antiferromagnetically" coupled to a methyl radical ($S = 1/2$), as seen in the case of the unligated complex. The reaction starts with a σ-attack of the methane σ_{CH} orbital to the Fe−O σ-bonding MOs. This interaction generates the $\sigma+\sigma_{CH}/\sigma-\sigma_{CH}$ bonding/antibonding pair of MOs shown in Figure 8 for the case of the unligated complex. On approaching the transition state the α-spin $\sigma-\sigma_{CH}$ orbital mixes with and transfers electron charge into the α-spin σ*. However, because of the hydrosulfide-induced upshift of this orbital, the mixing occurs at a shorter O−H distance than in the case of the unligated complex. This is why the transition state is reached later and features a barrier about two times higher than that computed for the unligated system (22.8 vs 11.7 kcal/mol). There is an additional factor contributing to the rise of the barrier, however. This is the weakening of the Fe−S bond because of population of the α-spin σ*, an Fe−O and Fe−S σ-antibonding MO (Figure 2). The weakening of the Fe−S bond is mirrored by the elongation of this bond on going from ^{5}**RC** to ^{5}**TS**$_{H_\sigma}$ (2.482 vs 2.574 Å, Table 7).

After passing the transition state the system forms the intermediate complex ^{5}**I**$_\sigma$, with a high-spin ($S = 5/2$) on the iron "antiferromagnetically" coupled to the methyl radical ($S = 1/2$).

Starting from ^{5}**I**$_\sigma$ the OH rebound step follows a π-mechanism through ^{5}**TS**$_{Reb_\pi}$. The remaining β-electron of the methyl radical is transferred to the weakly Fe−O antibonding β-spin π_X* MO. Consistent with a π-attack of the methyl radical, the Fe−O−C angle is in ^{5}**TS**$_{Reb_\pi}$ 135.8°. The transition state occurs relatively early, at a C−O distance of 2.271 Å, in agreement with a rather low (4.7 kcal/mol) barrier.

Similar to ^{3}**TS**$_{Reb_\sigma}$ and for the same electronic reasons, ^{5}**TS**$_{Reb_\pi}$ evolves toward the final reaction products, the methanol and the high-spin ($S = 2$) pentacoordinate Fe(II) hydrosulfide porphyrin derivative, ^{5}[Por(SH)Fe]$^-$, without forming a stable product complex. As inferred from the ΔE_p values in Table 5, ^{5}[Por(SH)Fe]$^-$ is 16.0 kcal/mol more stable than ^{3}[Por(SH)-Fe]$^-$, in agreement with experimental evidence indicating that pentacoordinate Fe(II) hydrosulfide porphyrin derivatives have a high-spin ground state.[29,30] The distinctive geometrical parameters computed for ^{5}[Por(SH)Fe]$^-$ compare very well with those experimentally determined for the high-spin [OEP(HS)Fe]$^-$ (OEP = octaethylporphyrinate) complex (see Figure 11).[29]

The horizontal approach of methane toward the Fe−O moiety in ^{5}**TS**$_{H_\pi}$ leads to a β-electron transfer from the substrate to the weakly Fe−O antibonding π_X* MO. The key geometrical parameters of ^{5}**TS**$_{H_\pi}$ (Table 7) closely resemble those obtained

Table 7. Bond Lengths (Å) and Bond Angles (deg) of the Key Local Minima and Transition States on the Quintet Surface for Methane Hydroxylation by [Por(SH)Fe^{IV}=O]$^-$

	^{5}**RC**	^{3}**TS**$_{H_\pi}$	^{5}**TS**$_{H_\sigma}$	^{5}**I**$_\pi$	^{5}**I**$_\sigma$	^{5}**TS**$_{Reb_\sigma}$	^{5}**TS**$_{Reb_\pi}$	^{5}[Por(SH)Fe]$^-$
Fe−O	1.659	1.806	1.809	1.873	1.926	1.947	1.991	
Fe−S	2.482	2.383	2.574	2.363	2.583	2.388	2.548	2.393
Fe−N[a]	2.089	2.087	2.094	2.070	2.097	2.089	2.094	2.167
O−H	2.409	1.112	1.112	0.967	0.965	0.966	0.963	
C−H	1.091	1.445	1.422	2.566	2.486			
C−O						2.261	2.271	
∠FeOH	170.0	118.6	148.2	110.0	116.2	106.1	111.8	
∠FeOC						158.1	135.8	
∠OHC	179.4	173.4	174.0	167.1	170.3			

[a]Average value.

dx.doi.org/10.1021/ic301232r | Inorg. Chem. 2012, 51, 9833−9845

for ^{3}**TS**$_{H_\pi}$ (Table 6). The hydrogen abstraction process on the quintet π-channel leads to the intermediate ^{5}**I**$_\pi$, where an intermediate spin (S = 3/2) Fe(III)-hydroxo complex is "ferromagnetically" coupled to a methyl radical. Starting from ^{5}**I**$_\pi$ the OH rebound step follows a σ-mechanism through ^{5}**TS**$_{Reb_\sigma}$, as seen on the triplet π-channel. In either case the remaining α-electron of the methyl radical is transferred to the α-spin σ^* MO of the catalyst and, consistently, a Fe−O−C angle of about 158° is computed for both, ^{5}**TS**$_{Reb_\sigma}$ and ^{3}**TS**$_{Reb_\sigma}$. The former is reached earlier and has a lower barrier than the latter (Tables 5−7), which is in line with the actual acceptor orbital, the α-spin σ^* being in ^{5}**TS**$_{Reb_\sigma}$ lower in energy than in ^{3}**TS**$_{Reb_\sigma}$. Similar to ^{5}**TS**$_{Reb_\pi}$, ^{5}**TS**$_{Reb_\sigma}$ evolves toward the final reaction products without forming a stable product complex. It should be noted, finally, that inclusion of solvation effects raises the rebound barriers by 4.4−4.8 kcal/mol (see Table 5). This is because, just as observed in the case of the unligated complex, solvation favors energetically the intermediate relative to the rebound transition state because of a larger solvent exposure of the former. The rise of the rebound barriers, however, does not change the ordering of the transition states, and the H-abstraction step remains the rate-determining step

CONCLUSIONS

The methane hydroxylation reaction by the PorFe^{IV}=O and [Por(SH)Fe^{IV}=O]$^-$ Cpd II mimics has been theoretically investigated on the ground triplet and excited quintet spin-state surfaces within the rebound mechanism scheme. On each spin surface both the σ- and π-channels have been explored.

It is found that the rate-determining step of the reaction is the H-abstraction, regardless of the catalyst and spin surface.

The H-abstraction reaction by PorFe^{IV}=O can proceed on the triplet surface either through the classic π-channel or through the nonclassical σ-channel, with the latter being favored. On the quintet surface the barrier could only be located for the classic σ-mechanism. The quintet σ-pathway encounters a much lower barrier than the triplet channels so that the quintet surface cuts through the triplet surfaces, thereby providing, in principle, a lower energy path for the reaction. Thus, a TSR mechanism with crossover from the ground state triplet surface to the quintet state surface is a plausible scenario for C−H bond activation by PorFe^{IV}=O.

As for the hydrosulfide-ligated complex, on the triplet surface the H-abstraction barrier could only be located for the classic π-mechanism, most likely because the Fe−O σ^* is too high in energy to make a σ-attack of the substrate favorable. On the quintet surface the H-abstraction reaction can proceed either through the classic σ-channel or the nonclassical π-channel, with the former being slightly favored. As the quintet surface lies above the triplet surface in the entrance channel of the oxidative process and is highly destabilized on both the σ-and π-pathways, a TSR mechanism with crossover from the ground state triplet surface to the quintet state surface is not a plausible scenario for C−H bond activation by [Por(SH)Fe^{IV}=O]$^-$ and the reaction can only occur on the triplet surface.

In the rebound step the second electron of the methane σ_{CH} orbital is transferred to an empty Fe−O σ^* or π^* MO of the Fe(III)-hydroxo complex. Depending on the nature of the actual acceptor orbital, the rebound process can proceed through a σ- or a π-pathway.

A detailed electronic structure analysis of the **TS**$_H$ species as well of the reactant complexes en route to the transition state provides insight into the electron transfer process accompanying the H-abstraction reaction. It is found that the electron transfer from the substrate σ_{CH} into the acceptor orbital of the catalyst occurs through a complex mechanism that is initiated by the interaction between the σ_{CH} and the low-lying, oxygen-rich Fe−O σ-bonding and/or Fe−O π-bonding orbitals of the catalyst.

On the triplet and quintet σ-pathways the methane σ_{CH} orbital interacts, initially, with the α- and β-spin components of the Fe−O σ-bonding MO. This *two-orbital four-electron* interaction generates the $\sigma+\sigma_{CH}$ and $\sigma-\sigma_{CH}$ bonding and antibonding pair of MOs, the σ_{CH} contribution being dominant in the latter. On approaching the transition state the α-spin component of the $\sigma-\sigma_{CH}$ mixes with and transfers charge into the σ^* leading to elongation of the Fe−O and C−H bonds.

On the triplet π-pathway the σ_{CH} orbital of the substrate interacts, initially, with both the Fe−O σ bonding and the Fe−O π bonding MOs of the catalyst. On approaching the transition state the resulting $(\sigma, \pi)-\sigma_{CH}$ antibonding combination mixes with and transfers charge into the empty Fe−O π_X^*.

Within the envisaged donor/acceptor interaction scheme, the efficiency of the H-abstraction process is mainly controlled by two electronic factors: (1) the energy match between the substrate σ_{CH} and the Fe−O σ-bonding and/or Fe−O π-bonding orbitals of the catalyst; (2) the energy of the acceptor orbital of the catalyst. The lower is the energy of this orbital, the earlier the mixing with the actual donor orbital occurs.

Thus, for a given substrate, the efficiency of the H-abstraction process can be improved by properly acting on the porphyrin substituents and/or on the axial ligand. This encourages the synergy between theory and experiment as a unique tool to design new and more reactive oxoiron(IV) porphyrin complexes.

AUTHOR INFORMATION

Corresponding Author

*E-mail: angela.rosa@unibas.it (A.R.), giampaolo.ricciardi@unibas.it (G.R.).

Notes

The authors declare no competing financial interest.

ACKNOWLEDGMENTS

We thank Prof. Evert Jan Baerends, Vrije Universiteit of Amsterdam and Pohang University of Science and Technology, for stimulating discussions. This research work was supported by the Università della Basilicata, Italy.

REFERENCES

(1) (a) Denisov, I. G.; Makris, T. M.; Sligar, S. G.; Schlichting, I. *Chem. Rev.* **2005**, *105*, 2253−2277. (b) Groves, J. T. In *Cytochrome P450: Structure, Mechanism, and Biochemistry*, 3rd ed.; Ortiz de Montellano, P. R., Ed.; Kluwer-Academic/Plenum: New York, 2005; (c) Ortiz de Montellano, P. R. *Chem. Rev.* **2010**, *110*, 932−948. (d) Sono, M.; Roach, M. P.; Coulter, E. D.; Dawson, J. H. *Chem. Rev.* **1996**, *96*, 2841−2887. (e) Nam, W. *Acc. Chem. Res.* **2007**, *40*, 522−531.

(2) (a) Krebs, C.; Fujimori, D. G.; Walsh, C. T.; Bollinger, J., J. M. *Acc. Chem. Res.* **2007**, *40*, 484−492. (b) Abu-Omar, M. M.; Loaiza, A.; Hontzeas, N. *Chem. Rev.* **2005**, *105*, 2227−2252. (c) Kryatov, S. V.; Rybak-Akimova, E. V.; Schindler, S. *Chem. Rev.* **2005**, *105*, 2175−2226.

(3) (a) Groves, J. T.; Haushalter, R. C.; Nakamura, M.; Nemo, T. E.; Evans, B. J. *J. Am. Chem. Soc.* **1981**, *103*, 2884−2886. (b) Nam, W.; Goh, Y. M.; Lee, Y. J.; Lim, M. H.; Kim, C. *Inorg. Chem.* **1999**, *38*, 3238−3240. (c) Fujii, H. *Coord. Chem. Rev.* **2002**, *226*, 51−60. (d) Ortiz de Montellano, P. R. *Cytochrome P450: Structure, Mechanism, and*

Biochemistry, 3rd ed.; Kluwer Academic/Plenum Publishers: New York, 2005; (e) Meunier, B.; de Visser, S. P.; Shaik, S. *Chem. Rev.* **2004**, *104*, 3947−3980.
(4) Groves, J. T. *Proc. Natl. Acad. Sci. U.S.A.* **2003**, *100*, 3569−3574.
(5) (a) Shaik, S.; Devesh, K.; de Visser, S. P.; Altun, A.; Thiel, W. *Chem. Rev.* **2005**, *105*, 2279−2328. (b) de Visser, S. P.; Tahsini, L.; Nam, W. *Chem.—Eur. J.* **2009**, *15*, 5577−5587. (c) Tahsini, L.; Bagherzadeh, M.; Nam, W.; de Visser, S. P. *Inorg. Chem.* **2009**, *48*, 6661−6669. (d) Altun, A.; Shaik, S.; Thiel, W. *J. Am. Chem. Soc.* **2007**, *129*, 8978−8987. (e) Hazan, C.; Kumar, D.; de Visser, S. P.; Shaik, S. *Eur. J. Inorg. Chem.* **2007**, *2007*, 2966−2974.
(6) (a) Nam, W.; Park, S.-E.; Lim, I. K.; Lim, M. H.; Hong, J.; Kim, J. *J. Am. Chem. Soc.* **2003**, *125*, 14674−14675. (b) Nehru, K.; Seo, M. S.; Kim, J.; Nam, W. *Inorg. Chem.* **2007**, *46*, 293−298. (c) Park, M. J.; Lee, J.; Suh, Y.; Kim, J.; Nam, W. *J. Am. Chem. Soc.* **2006**, *128*, 2630−2634.
(7) Groves, J. T.; Gross, Z.; Stern, M. K. *Inorg. Chem.* **1994**, *33*, 5065−5072.
(8) (a) Jeong, Y. J.; Kang, Y.; Han, A.-R.; Lee, Y.-M.; Kotani, H.; Fukuzumi, S.; Nam, W. *Angew. Chem., Int. Ed.* **2008**, *47*, 7321−7324. (b) Fukuzumi, S.; Kotani, H.; Lee, Y.-M.; Nam, W. *J. Am. Chem. Soc.* **2008**, *130*, 15134−15142.
(9) Bell, S. R.; Groves, J. T. *J. Am. Chem. Soc.* **2009**, *131*, 9640−9641.
(10) Groves, J. T.; McClusky, G. A. *J. Am. Chem. Soc.* **1976**, *98*, 859−861.
(11) Shaik, S.; Hirao, H.; Kumar, D. *Acc. Chem. Res.* **2007**, *40*, 532−542.
(12) de Visser, S. P. *J. Am. Chem. Soc.* **2006**, *128*, 15809−15818.
(13) Hirao, H.; Kumar, D.; Thiel, W.; Shaik, S. *J. Am. Chem. Soc.* **2005**, *127*, 13007−13018.
(14) Neidig, M. N.; Decker, A.; Choroba, O. W.; Huang, F.; Kavana, M.; Moran, G. R.; Spencer, J. B.; Solomon, E. I. *Proc. Natl. Acad. Sci. U.S.A.* **2006**, *103*, 12966−12973.
(15) Geng, C.; Ye, S.; Neese, F. *Angew. Chem., Int. Ed.* **2010**, *49*, 5717−5720.
(16) (a) Decker, A.; Rohde, J.-U.; Klinker, E. J.; Wong, S. D.; Que, L.; Solomon, E. I. *J. Am. Chem. Soc.* **2007**, *129*, 15983−15996. (b) Decker, A.; Chow, M. S.; Kemsley, J. N.; Lehnert, N.; Solomon, E. I. *J. Am. Chem. Soc.* **2006**, *128*, 4719−4733. (c) Hirao, H.; Kumar, D.; Que, L.; Shaik, S. *J. Am. Chem. Soc.* **2006**, *128*, 8590−8606. (d) Louwerse, M. J.; Baerends, E. J. *Phys. Chem. Chem. Phys.* **2007**, *9*, 156−166. (e) Michel, C.; Baerends, E. J. *Inorg. Chem.* **2009**, *48*, 3628−3638. (f) Hirao, H.; Que, L.; Nam, W.; Shaik, S. *Chem.—Eur. J.* **2008**, *14*, 1740−1756. (g) Rosa, A.; Ricciardi, G.; Baerends, E. J. *Inorg. Chem.* **2010**, *49*, 3866−3880. (h) Bernasconi, L.; Baerends, E. J. *Eur. J. Inorg. Chem.* **2008**, 1672−1681.
(17) Ye, S.; Neese, F. *Proc. Natl. Acad. Sci. U.S.A.* **2011**, *108*, 1228−1233.
(18) (a) Ahlrichs, R. *TURBOMOLE*, V6.3 2011; University of Karlsruhe and Forschungzentrum Karlsruhe GmbH; TURBOMOLE GmbH: Karlsruhe, Germany, 1989−2007; available from http://www.turbomole.com. (b) Ahlrichs, R.; Bär, M.; Häser, M.; Horn, H.; Kölmel, C. *Chem. Phys. Lett.* **1989**, *162*, 165−169.
(19) (a) Becke, A. D. *J. Chem. Phys.* **1993**, *98*, 5648−5652. (b) Lee, C.; Yang, W.; Parr, R. G. *Phys. Rev. B* **1988**, *37*, 785−789.
(20) Weigend, F.; Ahlrichs, R. *Phys. Chem. Chem. Phys.* **2005**, *7*, 3297−3305.
(21) (a) Gorelsky, S. I. *AOMix: Program for Molecular Orbital Analysis*; University of Ottawa: Ottawa, Canada, 2012; http://www.sg-chem.net/. (b) Gorelsky, S. I.; Lever, A. B. P. *J. Organomet. Chem.* **2001**, *635*, 187−196.
(22) (a) Klamt, A.; Schürmann, G. *J. Chem. Soc., Perkin Trans.* **1993**, *2*, 799−805. (b) Klamt, A. *J. Phys. Chem.* **1995**, *99*, 2224. (c) Klamt, A.; Jonas, V. *J. Chem. Phys.* **1996**, *105*, 9972−9981.
(23) Kumar, D.; Narahari Sastry, G.; de Visser, S. P. *J. Phys. Chem. B* **2012**, *116*, 718−730.
(24) (a) Kumar, D.; Hirao, H.; Que, L.; Shaik, S. *J. Am. Chem. Soc.* **2005**, *127*, 8026−8027. (b) Hirao, H.; Kumar, D.; Que, L., Jr.; Shaik, S. *J. Am. Chem. Soc.* **2006**, *128*, 8590−8606. (c) Janardanan, D.; Wang, Y.; Schyman, P.; Que, L., Jr.; Shaik, S. *Angew. Chem., Int. Ed.* **2010**, *49*, 3342−3345.
(25) Danovich, D.; Shaik, S. *J. Am. Chem. Soc.* **1997**, *119*, 1773−1786.
(26) Cheng, R. J.; Latos-Grazynski, L.; Balch, A. L. *Inorg. Chem.* **1982**, *21*, 2412−2418.
(27) Ye, S.; Neese, F. *Curr. Opin. Chem. Biol.* **2009**, *13*, 89−98.
(28) Ogliaro, F.; Harris, N.; Cohen, S.; Filatov, M.; de Visser, S. P.; Shaik, S. *J. Am. Chem. Soc.* **2000**, *122*, 8977−8989.
(29) Pavlik, J. W.; Noll, B. C.; Oliver, A. G.; Schulz, C. E.; Scheidt, W. R. *Inorg. Chem.* **2010**, *49*, 1017−1026.
(30) Caron, C.; Mitschler, A.; Riviere, G.; Ricard, L.; Schappacher, M.; Weiss, R. *J. Am. Chem. Soc.* **1979**, *101*, 7401−7402.